2012-8-21

Gain and Loss Mechanisms for Neutral Species in Low Pressure Fluorocarbon Plasmas by Infrared Spectroscopy

Caleb T. Nelson, *et al.*

JVSTA
JOURNAL OF VACUUM SCIENCE AND TECHNOLOGY A

Gain and loss mechanisms for neutral species in low pressure fluorocarbon plasmas by infrared spectroscopy

Caleb T. Nelson, Lawrence J. Overzet, and Matthew J. Goeckner

Citation: J. Vac. Sci. Technol. A **30**, 051308 (2012); doi: 10.1116/1.4746411
View online: http://dx.doi.org/10.1116/1.4746411
View Table of Contents: http://avspublications.org/resource/1/JVTAD6/v30/i5
Published by the AVS: Science & Technology of Materials, Interfaces, and Processing

Gain and loss mechanisms for neutral species in low pressure fluorocarbon plasmas by infrared spectroscopy

Caleb T. Nelson, Lawrence J. Overzet, and Matthew J. Goeckner[a)]
Department of Electrical Engineering, University of Texas at Dallas, P.O. Box 830688, Richardson, Texas 75083

(Received 6 March 2012; accepted 2 August 2012; published 21 August 2012)

This article examines the chemical reaction pathways of stable neutral species in fluorocarbon plasmas. Octafluorocyclobutane (c-C_4F_8) inductively coupled plasma discharges were found to primarily produce stable and metastable products downstream from the discharge, including c-C_4F_8, C_2F_4, C_2F_6, CF_4, C_3F_8, C_4F_{10}, C_3F_6, and CF_2. A novel analysis technique allows the estimation of gain and loss rates for neutral species in the steady state as functions of residence time, pressure, and discharge power. The gain and loss rates show that CF_4, C_2F_6, C_3F_8, and C_4F_{10} share related gain mechanisms, speculated to occur at the surface. Further analysis confirms that CF_2 is predominantly produced at the chamber walls through electron impact dissociation of C_2F_4 and lost through gas-phase addition reactions to form C_2F_4. Additionally, time-resolved FTIR spectra provide a second-order rate coefficient of 1.8×10^{-14} cm^3/s for the gas-phase addition of CF_2 to form C_2F_4. Finally, C_2F_4, which is much more abundant than CF_2 in the discharge, is shown to be dominantly produced through electron impact dissociation of c-C_4F_8 and lost through either surface or gas-phase addition reactions. © *2012 American Vacuum Society*. [http://dx.doi.org/10.1116/1.4746411]

I. INTRODUCTION

Fluorocarbon plasmas are frequently used because of their versatility and cost efficiency in surface modification processes. The flexibility of fluorocarbon plasma in treating silicon devices and polymer surfaces has led to a large number of publications attempting to understand the underlying process kinetics. Fundamental to this work is the early research of Coburn and Winters[1] in determining the synergistic effect of ions and neutrals in reactive ion etching, the demonstration of actinometric techniques for gas-phase species measurements by Coburn and Chen,[2] and the utilization of gas-phase measurements to discuss plasma–surface interactions by Donnelly *et al*.[3]

These works were quickly followed by a widespread effort to derive electron impact cross sections that has resulted in a variety of 0D global models[4–6] and hybrid multidimensional[7,8] models of plasmas to describe densities of neutral and charged particles as functions of power, pressure, and feed gas. While these models have been important in clarifying how breakdown processes and corresponding available radicals and ion fluxes might change under a variety of process conditions, there is still a need to understand gas-phase kinetics in more complex gases as well as surface driven processes and their impact on both the global and local partial pressures of plasma species.

To this end, numerous experimental investigations and numerical calculations have been undertaken. Fisher and co-workers[9–12] examined the interactions of radicals and surfaces showing the dominance of the ionic component. Graves and co-workers[13–15] extended the understanding of surface interaction through molecular dynamics simulations showing the importance of mixing layers. Oehrlein and co-workers[16,17] furthered the experimental understanding of mixing layers in reactive ion etching and demonstrated the effects of surface temperature. Booth and co-workers[18,19] used laser induced fluorescence and UV absorption to establish the production of CF and CF_2 on reactor walls, excluding them as dominant deposition precursors. Hayashi *et al*.[20] investigated kinetics in octafluorocyclobutane (c-C_4F_8) plasmas, concentrating on the production and loss of CF_2 and C_2F_4. Finally, Goeckner and co-workers[21–23] have explored the effect of chamber geometry on CF_4 and c-C_4F_8 plasmas.

The vast majority of both the experimental and computational research has long concentrated on the presence and activity of the smallest free radicals F, CF, CF_2, and CF_3 and their confluence with energetic ion species, which together have been thought to be the major contributors to surface deposition and etch processes.[24,25] Recently, it has been suggested that CF and CF_2 have a net gain from surfaces even in some heavily depositing conditions.[19,26,27] Only a few researchers have focused on the role of larger radicals in plasma–surface interactions.[28,29]

The bulk of the experimental research has relied on diagnostic techniques that are limited in their ability to detect unanticipated species. While both laser induced fluorescence and laser absorption spectroscopy provide excellent spatial and temporal measurements of radical species within the plasma, they are limited to examining wavelengths and species predetermined by the researcher. Mass spectrometry is more adept at probing plasmas for unexpected chemistries, but suffers from limitations in calculating absolute and relative densities among species. This technique also disturbs the surrounding plasma and can be compromised in heavily depositing plasmas. Fourier transform infrared (FTIR) spectroscopy provides a complementary approach that allows the detection of unanticipated species and the calculation of absolute densities. While FTIR is limited to line-averaged

[a)]Electronic mail: goeckner@utdallas.edu

densities and can be plagued by noise in unstable plasmas, it allows the simultaneous detection of most gas-phase chemistries with the exception of mono- and homodiatomic species. The technique of *in situ* FTIR spectroscopy has been used in fluorocarbon plasmas by multiple authors.[28–33] However, the conclusions concerning reaction kinetics have been limited because of incomplete spectral data and the difficulty in measuring electron energy distribution functions in heavily depositing plasmas.

This purpose of this article is to evaluate the major production and loss mechanisms for plasma species that are efficiently detected by the FTIR spectrometer, in order to provide quantitative data for plasma models. To this end, the experimental setup will be provided, followed by an examination of the relevant assumptions. Finally, the absolute species densities obtained from FTIR spectra will be analyzed to resolve potential reaction pathways for stable by-products. This will be accomplished by comparing the spectra of discharges with varying residence times, pressures, and powers.

II. EXPERIMENTAL SETUP

A brief description of the experimental setup and the diagnostic techniques used in this article will be provided, while more detail can be found elsewhere.[34] The experiments were performed in a modified Gaseous Electronics Conference (mGEC) reference cell,[35] as seen in Fig. 1. The specialized reactor is modified to study plasma–surface interactions by using variable electrode gaps, chamber diameters, wall materials, and wall temperatures. In this set of experiments, bead blasted bare aluminum walls of 20 cm diameter were used at room temperature, while a second aluminum disk, level with the movable source, created a ceiling. A third aluminum plate was used only during FTIR measurements to separate the discharge from the IR beam path, creating a dual residence time system. The outer region has a 100 l volume, while the inner region (a 10 cm × 10 cm cylinder) contains 3 l. A water-cooled five-turn inductive coil was used to couple the power to the plasma through a 1.27 cm alumina plate. The transmitted power of 400 W was kept constant at 13.56 MHz through a conventional L-type matching network. Discharge power was measured at the generator output so losses in the matching network and cables were ignored. Feed gas flowed into the chamber through a perforated 6 mm tube around the source bucket. A turbomolecular pump was placed underneath the bottom plate, and gas exited the system through slits around the outer diameter of the chamber and the lower electrode. c-C_4F_8 with a 10% argon addition was used as the feed gas. Flow conditions (15–60 SCCM) and pressures (6–45 mTorr) were chosen as a representation of common low-pressure plasma processing environments. (SCCM denotes cubic centimeters per minute at standard temperature and pressure.)

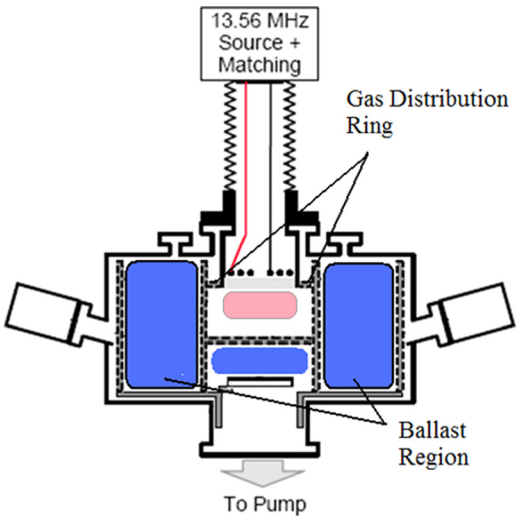

FIG. 1. (Color online) Schematic of the mGEC reactor used in experimentation (Ref. 35).

A number of diagnostic instruments were also used. Argon actinometry, in a technique first introduced by Coburn and Chen,[2] was used to obtain fluorine densities. Generally several conditions must be met in order to use actinometry. First, the emitting state of both actinometer and the reactive species must be predominantly excited through inelastic collisions of electrons with the ground state. In addition, the cross-sections for electron impact excitation of the two species must have similar electron energy thresholds. The 750.4 nm Ar emission has been the principal actinometer utilized in literature[2,36] for fluorine concentration measurements because of the close proximity of excitation energies (13.47 and 14.74 eV for Ar and F, respectively). A few authors[37,38] have questioned the validity of the 750.4 nm emission line at low powers and frequency ranges. We did not have the ability to validate the technique in our experimental setup. However, Savas[37] noted that at fixed frequency, and higher powers (larger high energy electron tail), the 750.4 nm line was preferable. The 750.4 nm Ar emission was compared to the 703.7 nm F emission, according to Eq. (1), where n_F and n_{Ar} are fluorine and argon densities, respectively, and I_F and I_{Ar} are emission intensities,

$$n_F = C_{F,Ar} n_{Ar} \frac{I_F}{I_{Ar}}. \quad (1)$$

The correction factor, $C_{F,Ar}$, related to the relative excitation cross sections, has been previously estimated[39] to be 0.6. The argon density was calculated from the flow rate and the residence time, assuming room temperature. For the actinometry measurement, a lens and fiber optic were used to collect emission from a 1 mm diameter spot 2 mm above the center of the platen.

A Jobin-Yvon *in situ* spectroscopic ellipsometer fixed at 633 nm was used to collect surface deposition rates. In addition, a WISE probe[40] using a 5 kHz signal was located in the center of the plasma, positioned at both 2 cm below the source and 2 cm above the bottom platen in order to reflect conditions in the plasma glow and near the deposition measurement. The WISE probe allowed the collection of ion densities and electron temperature without disturbance by the heavily depositing c-C_4F_8 plasma.

Finally, a Nicolet 870 Fourier-transform spectrometer was used in combination with a cryogenically cooled mercury–cadmium–telluride (MCT-A) detector. As seen in Fig. 2, the signal was passed multiple times through the chamber using a White cell[41] in order to increase the signal-to-noise ratio (SNR). The number of passes (4–24, corresponding to absorption path lengths of 3.25–19.5 m) was chosen to maximize the SNR, while limiting the maximum absorption of the peak being measured to 0.7 (20% transmittance) in order to fall within the linear regime of Beer's law. Appropriate cross sections for the application of Beer's law are published elsewhere.[42] Steady-state measurements were averaged across 64 scans with a mirror velocity of 4.7 cm/s and a resolution of 0.125 cm^{-1}. Time-dependent analysis was taken at 20 ms intervals, using a mirror velocity of 8 cm/s and a resolution of 8 cm^{-1}.

The gas temperature in inductively coupled plasmas can be significantly elevated above room temperature and greatly affect the IR absorption spectra as a result.[42] When the gas temperature is raised or varies with position, it makes a quantitative interpretation of FTIR spectra difficult at best. To address this difficulty and allow well calibrated, quantitative measurements of the various species in fluorocarbon plasmas, we employed a physical break between the plasma and the region probed by the FTIR beam. An aluminum plate placed between the plasma and the FTIR beam path, as seen in Fig. 1, allowed us to avoid the effects of elevated internal temperatures on discharge spectra. The volume outside of the cylinder containing the plasma is hereafter referred to as the ballast region. It is clearly the case that species which diffuse out of the plasma in the upper region to the FTIR beam path in the ballast region will not be highly reactive in either the gas phase or on walls. That said, FTIR measurements through the plasma region indicate that the vast majority of the gas-phase species already fit this description. However, important metastable species do diffuse to the ballast and lower region where they can be accurately measured.

Residence time of the plasma during steady-state conditions was measured by allowing the throttle valve to equilibrate the plasma to a given pressure. At steady state, the angle of the throttle valve was locked and the coil power turned off. The new pressure was used to calculate the residence time according to Eq. (2), where p_{post_plasma} is the pressure measured after the power is turned off, $V_{chamber}$ is the volume of the chamber, and Q is the flow rate of the feed gas,

$$\tau_{res} = \frac{p_{post\_plasma} V_{chamber}}{Q}. \tag{2}$$

These conditions lead to long residence times for the entire volume, ranging from 3 to 17 s. A conservative estimate of the maximum diffusion loss time (τ_D) for all species is calculated using Eq. (3),[43] where 40 cm is used for Λ_0 (the characteristic length), and the diffusivity, $D_{C_xF_y}$, is calculated for transport through C_4F_8,

$$\tau_D = \frac{\Lambda_0^2}{D_{C_xF_y}} \leq 0.35\,\text{s}. \tag{3}$$

Because $\tau_D \ll \tau_{res}$, all species in the FTIR beam path that do not have significant loss rates in the ballast area should be distributed equally. (That is to say, those species should have a nearly constant density throughout the reactor.) This greatly simplifies the line-averaged FTIR analysis.

III. RESULTS AND ANALYSIS

Accurate interpretation of FTIR spectra is useful because it provides absolute densities for a large number of species. Steady-state densities can then be used in determining gain (G) and loss (L) mechanisms for each of the species. In this section, the continuity equation will be applied to globally analyze steady-state densities. This will be accomplished by systematically establishing dominant production and loss

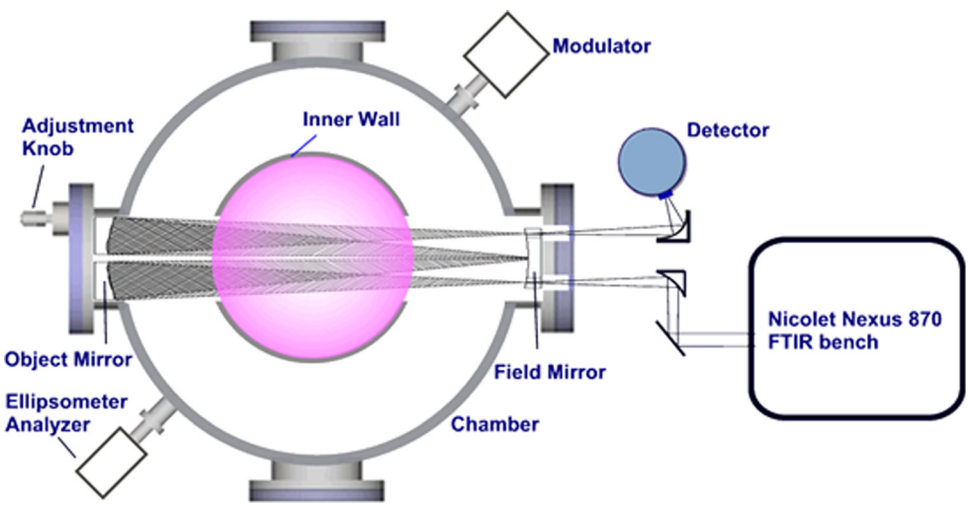

FIG. 2. (Color online) Schematic of the FTIR and White cell used in experimentation (Ref. 41).

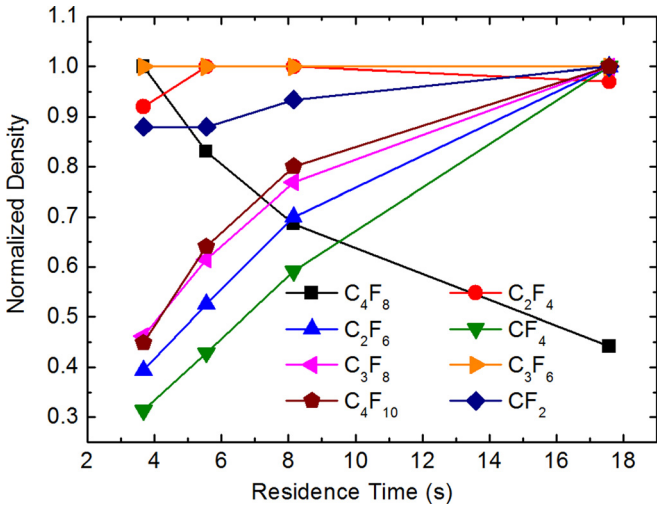

FIG. 3. (Color online) Normalized density of FTIR species as a function of residence time. The normalization factors are c-C_4F_8, $3.89 \times 10^{14}\,cm^{-3}$; C_2F_4, $3.48 \times 10^{14}\,cm^{-3}$; C_2F_6, $1.36 \times 10^{14}\,cm^{-3}$; CF_4, $1.14 \times 10^{14}\,cm^{-3}$; C_3F_8, $3.52 \times 10^{13}\,cm^{-3}$; C_3F_6, $1.62 \times 10^{13}\,cm^{-3}$; C_4F_{10}, $9.75 \times 10^{12}\,cm^{-3}$; CF_2, $6.09 \times 10^{13}\,cm^{-3}$.

pathways and the ensuing quantitative values for each type of production and loss. To this end, steady-state densities for FTIR species under a variety of conditions will be presented in tandem with localized measurements of ion flux, electron temperature, fluorine density, and deposition rates. Species with the simplest gain and loss mechanisms (c-C_4F_8) will be analyzed first. Established gain and loss rates will then be applied to species with more complex processes. For each of the species these rates will be considered as functions of residence time, gas pressure, and plasma power in order to validate the applied assumptions and discuss the dominant mechanism behind the gain and loss rates.

Mathematically, the spatially independent continuity equation for a given species is represented by

$$\frac{d}{dt}C_xF_y = G - L = 0. \tag{4}$$

Gain and loss processes can be expanded into several channels. These have been outlined in detail previously.[44] The net gain for a species can be written as

$$G = G_{\text{feed gas}} + G_{\text{elect}} + G_{\text{sputter}} + G_{\text{wall}} + G_{\text{react}} + G_{\text{charge exchange}}, \tag{5}$$

where $G_{\text{feed gas}}$ refers to gain directly from the feed gas, G_{elect} is gain due to electron impact on parent species, G_{sputter} is gain from ion induced sputtering off of chamber walls, G_{wall} is gain from chemical reactions on chamber walls, G_{react} is gain from polymerization in the gas phase, and $G_{\text{charge exchange}}$ is gain from charge exchange collisions. Similarly, net loss for a species can be written as

$$L = L_{\text{elect}} + L_{\text{charge exchange}} + L_{\text{pump}} + L_{\text{wall}} + L_{\text{react}}, \tag{6}$$

where L_{elect} is loss due to electron impact, $L_{\text{charge exchange}}$ is loss due to charge exchange collisions, L_{pump} is loss to the pump, L_{wall} is loss to chamber surfaces, and L_{react} is loss due to gas-phase polymerization reactions.

The relative magnitudes of these reaction channels can be changed with external controls. Figures 3–8 show the change in steady-state densities of neutral radicals, electron temperature, ion flux, fluorine density, and deposition rate as functions of residence time, pressure, and power. The residence time was varied from 3 to 17 s in Figs. 3 and 4 by keeping the pressure constant and decreasing the flow rate of c-C_4F_8

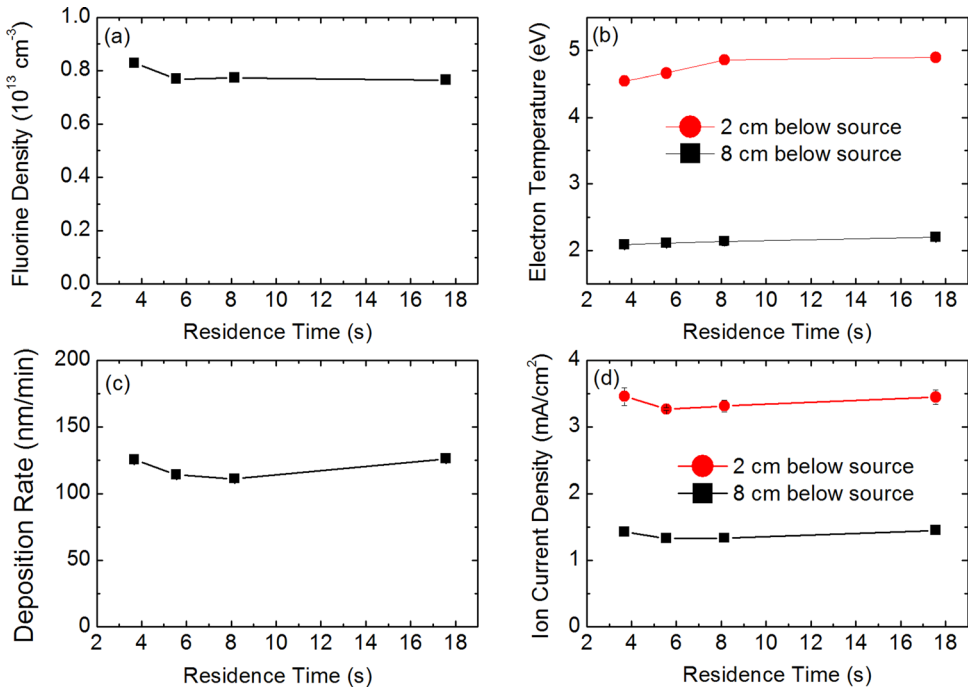

FIG. 4. (Color online) (a) Fluorine density, (b) electron temperature, (c) deposition rate, and (d) ion current as functions of residence time.

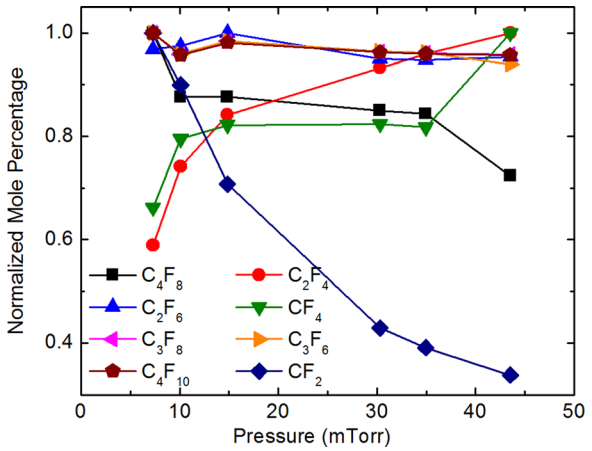

FIG. 5. (Color online) Normalized mole percentage of FTIR species as a function of discharge pressure. The normalization factors are c-C_4F_8, 33.8%; C_2F_4, 34.7%; C_2F_6, 10.7%; CF_4, 6.85%; C_3F_8, 2.44%; C_3F_6, 1.01%; C_4F_{10}, 0.70%; CF_2, 1.35%.

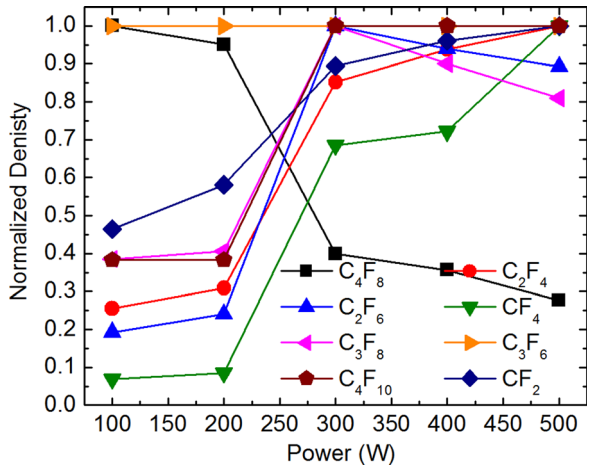

FIG. 7. (Color online) Normalized density of FTIR species as a function of discharge power. The normalization factors are c-C_4F_8, $7.87 \times 10^{14}\,cm^{-3}$; C_2F_4, $3.52 \times 10^{14}\,cm^{-3}$; C_2F_6, $1.06 \times 10^{14}\,cm^{-3}$; CF_4, $7.88 \times 10^{13}\,cm^{-3}$; C_3F_8, $2.47 \times 10^{13}\,cm^{-3}$; C_3F_6, $9.56 \times 10^{12}\,cm^{-3}$; C_4F_{10}, $8.09 \times 10^{12}\,cm^{-3}$; CF_2, $5.76 \times 10^{13}\,cm^{-3}$.

gas into the chamber from 60 to 15 SCCM. This change primarily affects the gain rate of the feed gas and the pump loss rate. Figure 4 shows that important parameters such as electron temperature, ion flux, and fluorine density do not change significantly with residence time. Deposition rate also remains approximately constant even though the percentage of c-C_4F_8 that is dissociated increases with residence time. Examination of the gain and loss mechanisms for each species might yield some information about the reason for this phenomenon. It is interesting to observe that while the densities of CF_4, C_2F_6, C_3F_8, and C_4F_{10} increase with increasing residence time, the densities of CF_2, C_2F_4, and C_3F_6 remain approximately constant as the residence time changes.

The pressure was also varied in Figs. 5 and 6 while holding the residence time constant at approximately 8 s by increasing the flow rate proportionally to the pressure. Small variations in residence time (<0.2 s) occurred due to minor changes in breakdown of the parent gas and the net deposition rate at different pressures. Increasing the pressure increases the total amount of radicals in the system, increasing all gains and losses with first- and second-order dependence; however, the time each molecule is exposed to the plasma remains approximately constant, as evidenced by the unchanging mole percentage of chemically stable species in Fig. 5.

Finally, the net power was varied from 100 to 500 W in Figs. 7 and 8. Here the energy per molecule changes significantly while the residence time and pressure are held constant. A distinct change in the plasma can be observed as it transforms from a capacitively coupled plasma to an

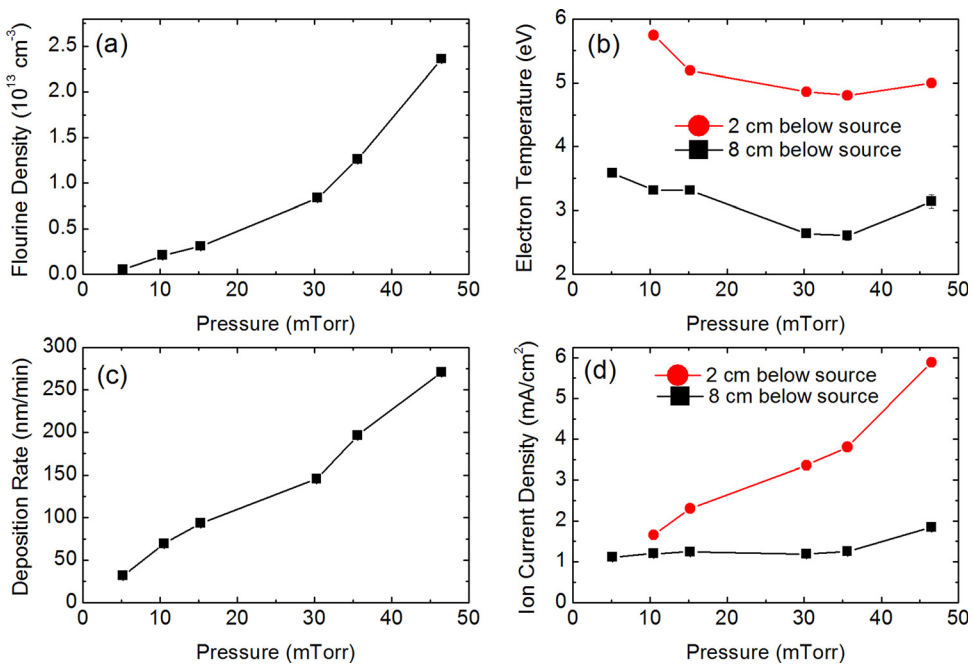

FIG. 6. (Color online) (a) Fluorine density, (b) electron temperature, (c) deposition rate, and (d) ion flux as functions of pressure.

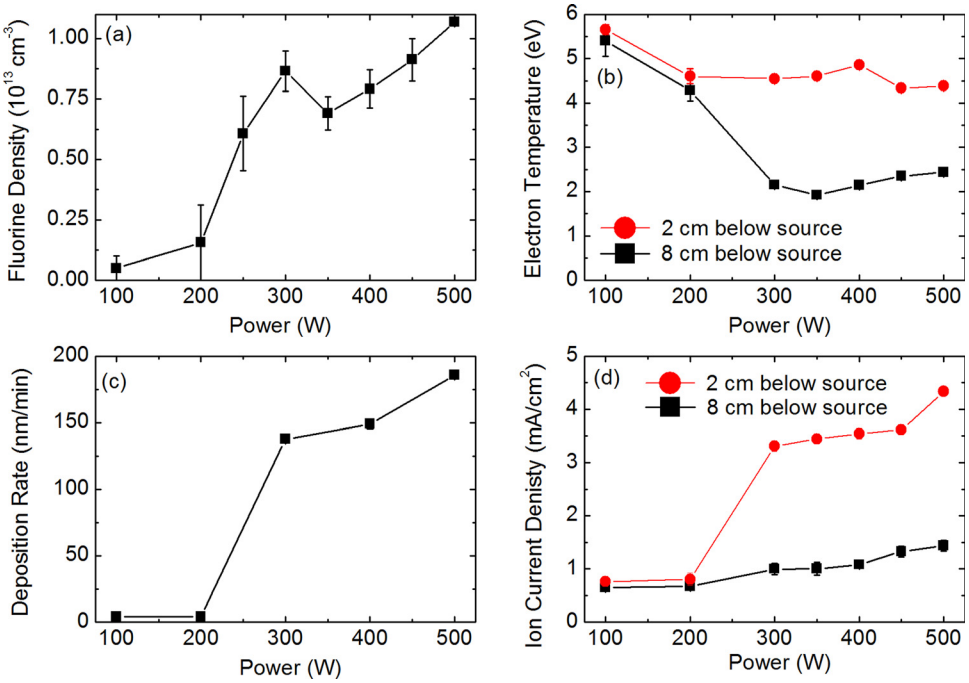

FIG. 8. (Color online) (a) Fluorine density, (b) electron temperature, (c) deposition rate, and (d) ion flux as functions of discharge power.

inductively coupled plasma. The density of all product species increases as the power is raised. However, the rate of increase varies with each species and is largely a function of the type of power coupling.

A. Gain and loss mechanisms for *c*-C_4F_8

Analysis of the gain and loss processes contributing to the aforementioned steady-state values will begin with the parent gas, *c*-C_4F_8. Only gain from the feed gas is considered because the formation of *c*-C_4F_8 either through gas-phase polymerization or as a surface product is unlikely to be significant due to the energy of formation. Losses due to ion impact dissociation or electron attachment are small in magnitude compared to pump loss and electron impact dissociation.[5] With this reasoning, the continuity equation for *c*-C_4F_8 steady-state density can be simplified to

$$G_{\text{feed gas}} - L_{\text{elect}} - L_{\text{pump}} = Q - n_{C_4F_8}\left[\frac{T_{\text{ballast}}}{T_{\text{plasma}}} V_{\text{plasma}} k_{C_4F_8} n_e + \frac{V_{\text{chamber}}}{\tau_{\text{res}}}\right] = 0. \quad (7)$$

Here, Q is the flow rate of the feed gas, $n_{C_4F_8}$ is the line-averaged *c*-C_4F_8 density in the ballast region, V_{plasma} is the plasma volume, V_{chamber} is the chamber volume, n_e is the electron density, T_{ballast} is the gas temperature in the ballast region, T_{plasma} is the gas temperature in the plasma, and $k_{C_4F_8}$ is the integrated total dissociation cross section. The residence time is inversely related to the flow rate by the equation $\tau_{\text{res}} = pV_{\text{chamber}}/Q$, where p is the chamber pressure.

The gain and loss rates of *c*-C_4F_8 as functions of residence time can be seen in Fig. 9. The gain rate is calculated from the input flow of fresh gas. The pump loss rate, L_{pump}, is calculated from the measured *c*-C_4F_8 density and the set chamber residence time. The difference between the gain and the pump loss is attributed to the electron impact loss rate, L_{elect}. Figure 4 shows that residence time does not have a significant effect on either the ion flux or the electron temperature. It is expected that the electron density and electron-impact dissociation cross sections are also unaffected by the gas residence time. A 10% decrease in the ratio of L_{elect} to $n_{C_4F_8}$ occurs as the residence time increases. This is due to the location of the gas inlet. At small residence times and the corresponding large flow rates, a higher partial pressure of the parent gas remains around the gas inlet, allowing for a slight increase in electron impact dissociation. However, as the flow rate is decreased to 30 SCCM (corresponding to $\tau_{\text{res}} = 8$), this effect becomes unimportant.

Figures 10 and 11 show the gain and loss rates of *c*-C_4F_8 as functions of discharge pressure and power. Predictably, the electron impact loss rate increases as both pressure and power are increased; however, the product $(T_{\text{ballast}}/T_{\text{plasma}})$ $V_{\text{plasma}} k_{C_4F_8} n_e = L_{\text{elect}}/n_{C_4F_8}$ appears to remain approximately constant across the pressure range of interest. Because of the complexity of the term, it is difficult to compare this measurement to the point measurements of ion density in Fig. 10; however, the significant shift between 35 and 45 mTorr corresponds to a shift in the power coupling. The electron impact loss rate also shifts dramatically between 200 and 300 W of net power. This occurs as the *H* mode becomes dominant at higher powers.

B. Gain and loss mechanisms for CF_4, C_2F_6, C_3F_8, and C_4F_{10}

We also investigated the generation and loss processes of stable neutral species such as CF_4, C_2F_6, C_3F_8, and C_4F_{10}. These molecules are all fully saturated structures so it is unlikely that they will be created through direct electron

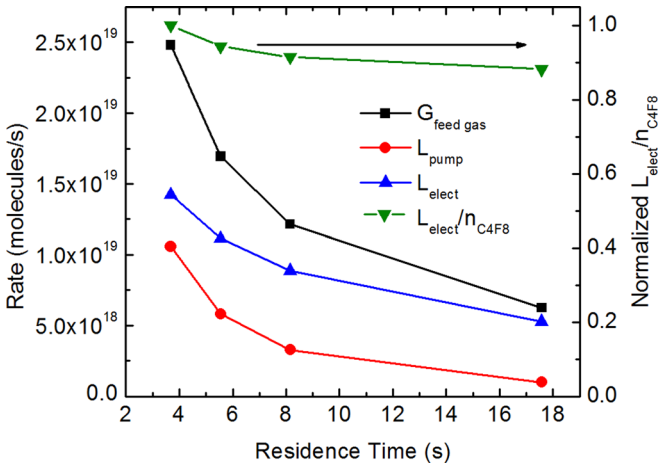

FIG. 9. (Color online) Gain and loss rates of c-C_4F_8 as a function of residence time.

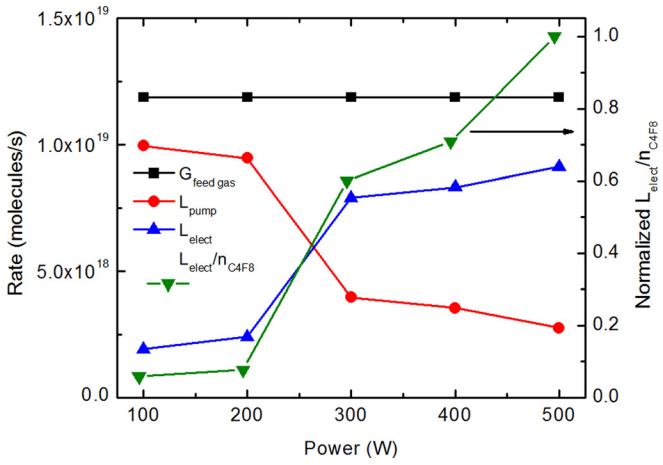

FIG. 11. (Color online) Gain and loss rates of c-C_4F_8 as a function of power.

impact dissociation of c-C_4F_8 or its by-products. Thus, the majority of the gain must come through desorption reactions off of chamber surfaces or gas-phase reactions. Significant loss channels can be limited to pump loss and electron impact dissociation and ionization, allowing their steady-state density to be defined according to

$$G_{\text{wall}} + G_{\text{react}} - L_{\text{pump}} - L_{\text{elect}} = 0. \tag{8}$$

A rough estimate of L_{elect} can be derived from the electron loss rate calculated for c-C_4F_8 by comparing the relative total dissociation cross sections for the various species,

$$L_{\text{elect\_}C_xF_y} = \frac{L_{\text{elect\_}C_4F_8}}{n_{C_4F_8}} \frac{k_{C_xF_y}}{k_{C_4F_8}} n_{C_xF_y}. \tag{9}$$

It is worth noting that some additional error will be introduced by varying values of diffusivity. Total dissociation cross sections were calculated for CF_4,[44] C_2F_6,[45] and C_3F_8 (Ref. 46) by integrating cross sections taken from literature across a Maxwellian energy distribution. Because total dissociation cross sections were unavailable, the sum of the neutral dissociation and ionization cross sections is used for C_2F_4 (Ref. 47) and c-C_4F_8.[48,49] Although the absolute error for cross sections can be large in some cases, only the relative error affects the estimate of electron impact loss. The total values for each molecule are primarily provided by two groups using similar methods so the relative error was estimated as $\pm 20\%$. The integrated cross sections as functions of electron temperature are compiled in Fig. 12 with the exception of C_4F_{10}, for which no cross-section information was available. The sum of the pump loss rate and the electron loss rate calculated using these values is equated to the net gain rate for each of the species.

Production and loss rates for each species have been plotted as a function of residence time in Fig. 13. Significantly, the calculated gain rates do not vary appreciably as the residence time of the species increases. This result accords well with expectations that these species must be created either at the wall or through gas-phase reactions. Thus, the gain rates are expected to increase as a function of either the ion flux to the surface or the density of potential gas-phase reactants, but not as a function of the residence time. Figures 3 and 4

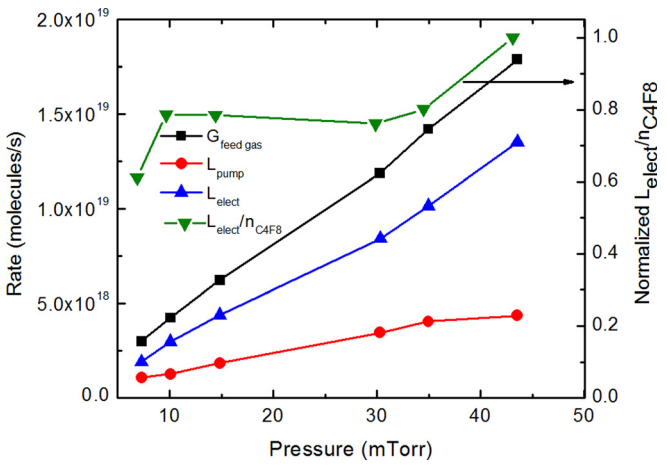

FIG. 10. (Color online) Gain and loss rates of c-C_4F_8 as a function of pressure.

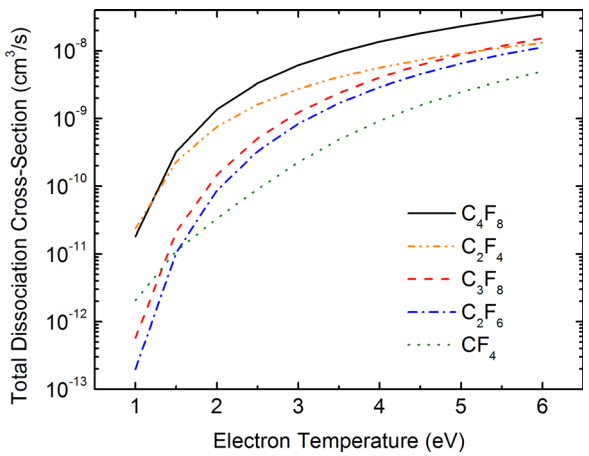

FIG. 12. (Color online) Estimated total dissociation cross sections as a function of electron temperature for c-C_4F_8 (Refs. 48 and 49), C_2F_4 (Ref. 47), C_3F_8 (Ref. 46), C_2F_6 (Ref. 45), and CF_4 (Ref. 44).

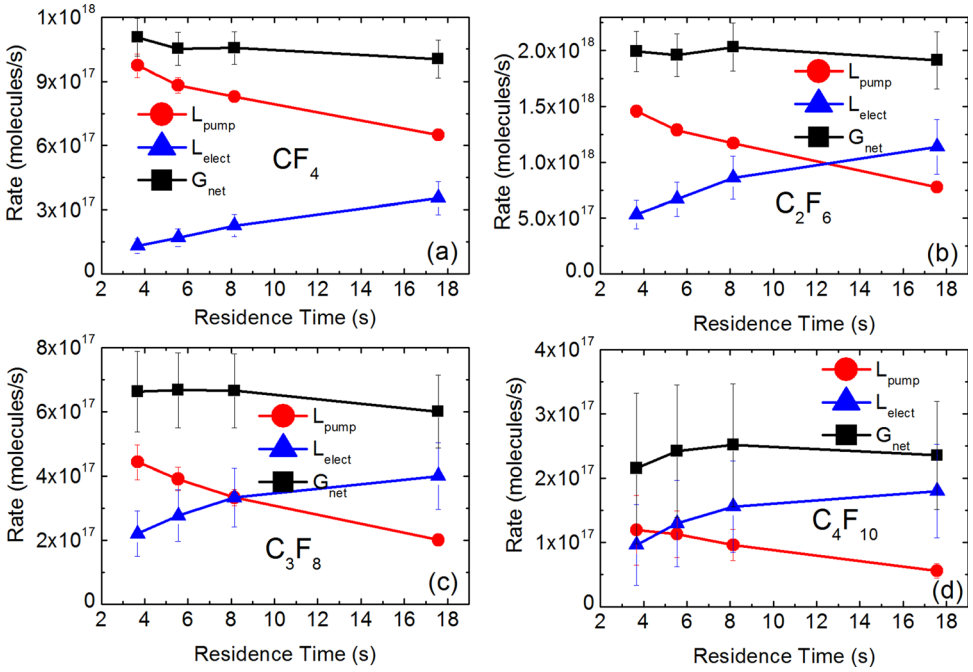

FIG. 13. (Color online) Gain and loss rates for (a) CF_4, (b) C_2F_6, (c) C_3F_8, and (d) C_4F_{10} as functions of residence time.

show that neither the ion current density nor potential gas-phase reactants (F, CF_2, C_2F_4) change significantly with residence time. A total dissociation cross section of $1.38 \pm 0.4 \times 10^{-8}$ for C_4F_{10} was estimated in order to maintain a constant gain rate. Of interest is the fact that C_2F_6 has a larger production rate than CF_4 even though it is rarely considered in plasma models.

As the gas pressure is increased both the loss to electron impact and the loss to the pump increase, almost solely as a function of the increased density of the species (see Fig. 14). This leads to approximately linear increases in gain rates as pressure increases. Normalizing the gain rates in Fig. 15 shows that the ratio of production rates among species remains approximately constant. This consistency indicates that the species are being produced through similar reaction channels, while also affirming the validity of the analysis and the cross sections from literature. It is important to notice that the gain rates scale proportionately with both the deposition rate on the chuck and the ion flux near the source, which differs from the ion flux to the chuck. This leads to a couple of tentative conclusions. First, it indicates that these products are likely produced by addition reactions on the surface,

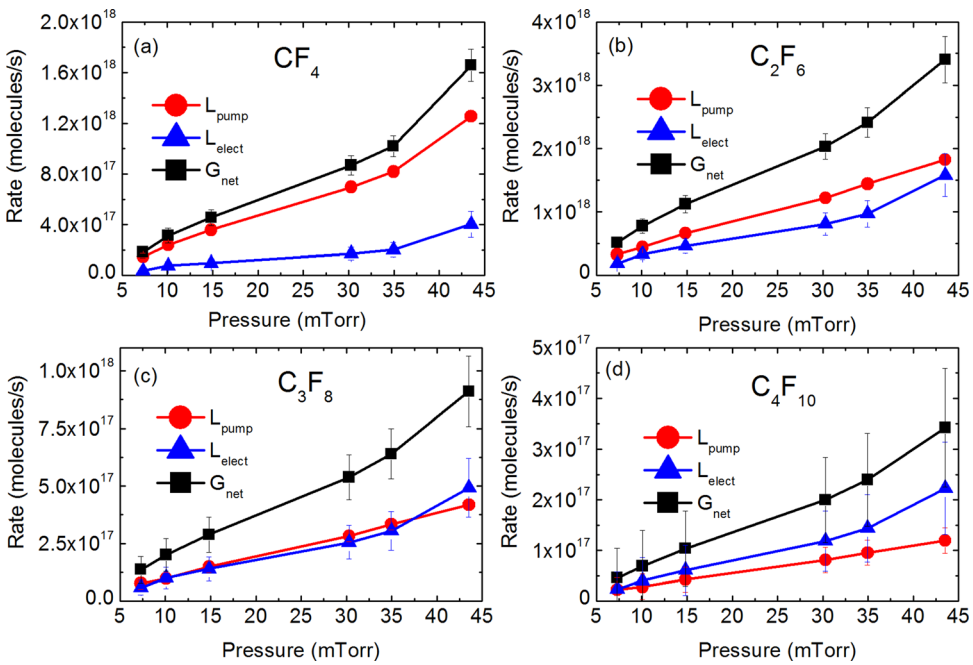

FIG. 14. (Color online) Gain and loss rates for (a) CF_4, (b) C_2F_6, (c) C_3F_8, and (d) C_4F_{10} as functions of pressure.

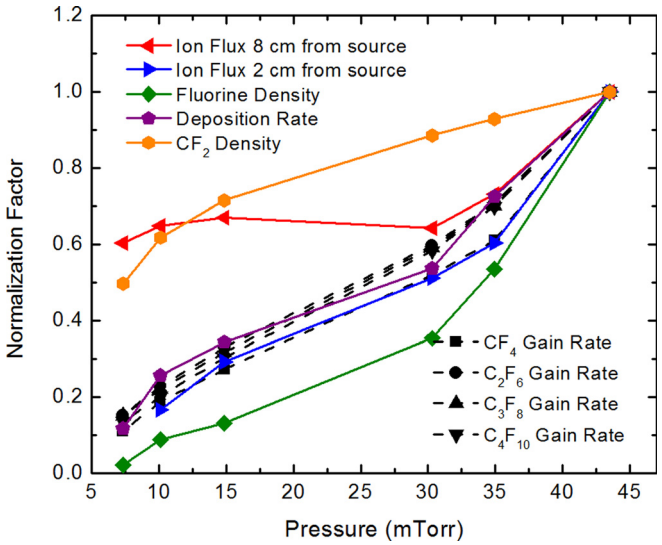

FIG. 15. (Color online) Gain rates of CF_4, C_2F_6, C_3F_8, and C_4F_{10} as a function of pressure, compared to ion fluxes measured at the source and chuck and the deposition rate at the chuck.

which are fueled by either radicals desorbing from the surface through the influence of ion impact or neutralized ion fragments. This surface would then provide a pathway for energy and momentum conservation in the exothermic addition reactions without the need for a third body in the gas phase or the production of hot neutrals, both of which drastically reduce the probability of the addition reaction,[43] as can be seen by analyzing the standard enthalpy of reaction for CF_4,

$$\mathrm{CF_3}(-4.94\,\mathrm{eV}) + \mathrm{F}(0.82\,\mathrm{eV}) \rightarrow \mathrm{CF_4}(-9.59\,\mathrm{eV}) + 5.47\,\mathrm{eV}. \quad (10)$$

Equation (10) indicates that the production of CF_4 is an exothermic reaction producing 5.5 eV. This can be compared to approximate energy of a C–F bond on CF_4 (~5.6 eV).[50] While it is possible for this reaction to occur in the gas phase, the resultant product is unstable. Lieberman and Lichtenberg[43] have estimated the average radiative lifetime for electric dipole radiation to be 10^{-9}–10^{-8} s and the dissociation time of an unstable molecular state to be 10^{-12}–10^{-13} s, causing the overall rate of the production of the molecule to be low unless it is formed on a surface where energy can be dissipated. Although the enthalpies of formation are not known for all possible reagents for the other species, it is expected that their corresponding reaction will have similar energies of formation, indicating the likelihood of a surface driven reaction.

Second, the observation that the gain rates increase on the same scale as the ion flux at the source and not that at the chuck indicates that only the surfaces close to the source (i.e., dielectric window) are important in determining the gain rates. This is important because the dielectric window is much more difficult to maintain at an equilibrated temperature, leading to time hysteresis effects in processing. Finally, it is interesting to observe that the deposition rate on the chuck scales proportionately to the ion flux near the source rather than the ion flux near the chuck. This could be explained by the hypothesis that heavy mass species forming on the source window can be desorbed by ion bombardment and subsequently redeposit on remote surfaces despite a smaller ion flux there.[19] It is important to note that this is not conclusive proof as to the source of the neutrals, as both CF_2 and F (possible precursors for gas-phase addition reactions) also increase with pressure, albeit not at the same rate. Additionally, both the CF_2 and F measurements were taken downstream, and it is difficult to predict local densities in the plasma volume. This is particularly true for F, which will have a much faster loss rate as the mean free path decreases, leading to a larger difference between the F density in the plasma volume and the density measured at the chuck surface.

Gain and loss rates for CF_4, C_2F_6, C_3F_8, and C_4F_{10} are also plotted in Fig. 16 as a function of discharge power. The gain rates vary only weakly as a function of power when the discharge is in *H* mode or *E* mode, although there is a large disparity between the two modes. The normalized gain rates in Fig. 17 again scale closely with the ion flux to the source. However, as power increases the production channel favors lower mass species. The reaction pathway must occur through some combination of Eqs. (11)–(13) either on a surface or in the gas phase,

$$\mathrm{C}_a\mathrm{F}_{2a} + \mathrm{C}_b\mathrm{F}_{2b} \rightarrow \mathrm{C}_c\mathrm{F}_{2c}, \quad (11)$$

$$\mathrm{C}_c\mathrm{F}_{2c} + \mathrm{C}_d\mathrm{F}_{2d+1} \rightarrow \mathrm{C}_f\mathrm{F}_{2f+1}, \quad (12)$$

$$\mathrm{C}_f\mathrm{F}_{2f+1} + \mathrm{C}_e\mathrm{F}_{2e+1} \rightarrow \mathrm{C}_g\mathrm{F}_{2g+2}. \quad (13)$$

Thus ignoring changes in collision cross sections, the relative gain rates can be approximately defined as in Eq. (14), where $\bar{x}$ and $\bar{y}$ are the average number of carbon atoms in each type of radical,

$$\frac{G_{\mathrm{C}_{n+1}\mathrm{F}_{2n+4}}}{G_{\mathrm{C}_n\mathrm{F}_{2n+2}}} \propto \frac{[\mathrm{C}_{\bar{x}}\mathrm{F}_{2\bar{x}}]}{[\mathrm{C}_{\bar{y}}\mathrm{F}_{2\bar{y}+1}]}. \quad (14)$$

This means that in order to produce lower mass species, the ratio of $[\mathrm{C}_{\bar{x}}\mathrm{F}_{2\bar{x}}]/[\mathrm{C}_{\bar{y}}\mathrm{F}_{2\bar{y}+1}]$ must decrease. We only have partial measurements for the localized densities of the smallest two species of each representative type of molecule so caution must be used in extrapolating spatial dependent distributions. In addition, it is likely that these reactions occur through the surface film, and the ratio $[C_{\bar{x}}F_{2\bar{x}}]/[C_{\bar{y}}F_{2\bar{y}+1}]$ could be significantly different at the surface. However, it can be seen that the CF_2/F ratio increases as power decreases due to the decrease in electron impact dissociation, leading to a possible explanation for the increase in the average number of carbon atoms in the gain of the neutral species. A more thorough investigation is needed to corroborate this explanation.

C. CF_2 production and loss mechanisms

The production and loss of CF_2 has been a topic of interest for more than a decade, with some research concluding that it is a primary precursor for deposition, while others have concluded that it is primarily formed at the surface.

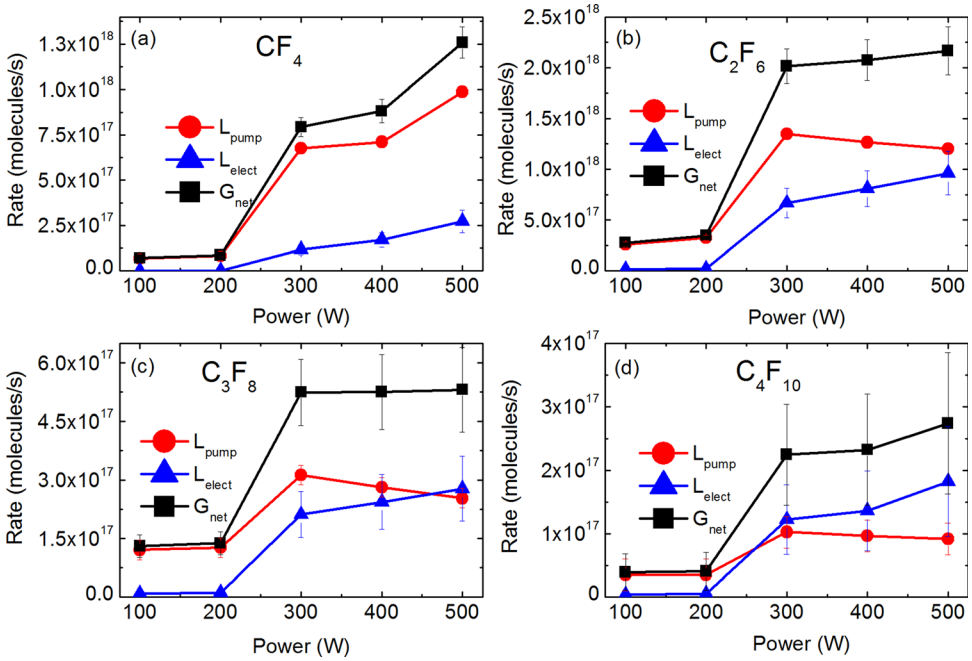

FIG. 16. (Color online) Gain and loss rates for (a) CF_4, (b) C_2F_6, (c) C_3F_8, and (d) C_4F_{10} as functions of coil power.

Unlike the stable species previously discussed, CF_2 can include significant gain and loss mechanisms both outside of the plasma glow and on the wall because of the presence of unpaired electrons. Thus, a larger gain and loss set must be considered in balancing the CF_2 density. While gain from sputtering can be ignored at low ion energies ($\sim$20 eV), gain from neutralized ion fragments will be included as part of the wall gain. Additionally, charge exchange gains and losses will be ignored, leading to a steady-state continuity equation described by

$$\frac{d[CF_2]}{dt} = G_{elect} + G_{wall} + G_{react} - L_{elect} - L_{pump} - L_{wall} - L_{react} = 0. \quad (15)$$

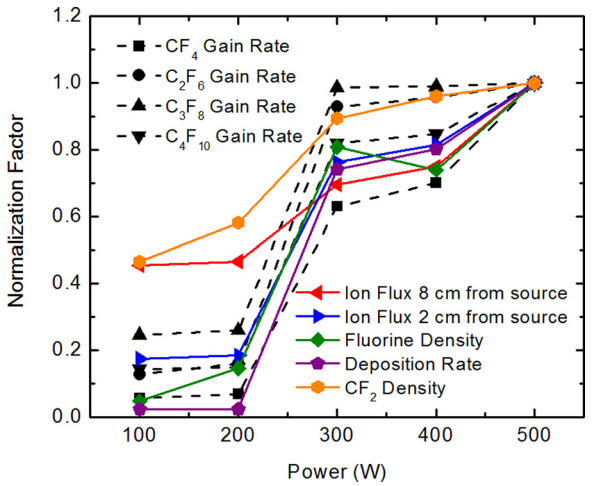

FIG. 17. (Color online) Normalized gain rates of CF_4, C_2F_6, C_3F_8, and C_4F_{10} as a function of power, compared to ion flux, F density, CF_2 density, and deposition rate.

Loss rates to the pump and to electron impact reactions can be calculated in the same way as Eqs. (7) and (9). The gain rate from electron impact reactions can be estimated as predominately coming from

$$C_2F_4 + e \rightarrow CF_2 + CF_2 + e. \quad (16)$$

Parameterized rate coefficients for this reaction are available in literature[49] and can be related to the loss rate of c-C_4F_8 to calculate a gain rate for CF_2 as in the following:

$$G_{elect\_CF_2} = \frac{L_{elect\_C_4F_8}}{n_{C_4F_8}} \frac{k_{C_2F_4 \rightarrow CF_2}}{k_{C_4F_8}} n_{C_2F_4}. \quad (17)$$

Finally, the predominant loss rate to gas-phase reactions can be calculated by observing time-resolved FTIR densities. These densities are plotted in Fig. 18. All of the densities with the exception of CF_2 are predominantly controlled by the residence time of the system because no reactions occur in the ballast area, so the c-C_4F_8 already there must first be displaced by pump loss. However, the CF_2 density increases rapidly and settles within 2 s of plasma ignition. We will discuss the possible reasons for this after solving the continuity equation. Loss in CF_2 can be seen as a function of time after the plasma is turned off and the gas contained. The product is easily identified because of the corresponding increase in C_2F_4 density, leading to the conclusion that Eq. (18) dominates the loss process of CF_2,

$$CF_2 + CF_2 \rightarrow C_2F_4. \quad (18)$$

Although reactions with F and C_xF_y are likely, their densities in the ballast region are low, while that of CF_2 remains relatively high. No other increases in density after the plasma is turned off are measurable with the FTIR data, leading to the

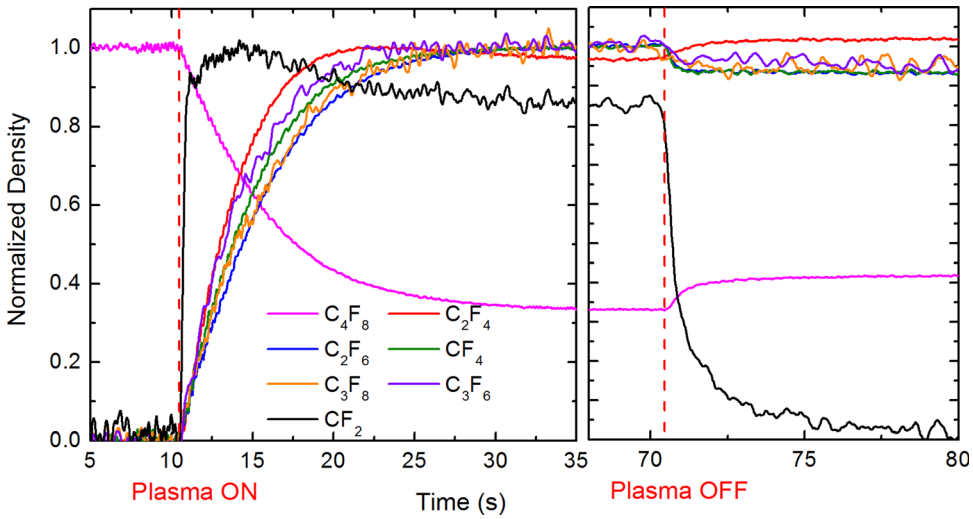

FIG. 18. (Color online) Normalized densities in a c-C_4F_8 discharge as a function of time.

conclusion that Eq. (18) accounts for >80% of the CF_2 loss. This reaction could take place on the wall or in the gas phase as a two-body or three-body reaction. Reactions on the wall will display first-order dependence as in Eq. (13), while reactions in the gas phase will display second-order dependence as in Eq. (11). If a three-body reaction dominates, then a pressure dependence will exist. The decay rate was fit for four different pressures according to

$$\frac{d[CF_2]}{dt} = \frac{1}{k_{cf2\rightarrow c2f4}t + [CF_2]_0^{-1}}. \tag{19}$$

The value of $k_{cf2\rightarrow c2f4}$ was found to be constant with pressure, having an average value of $1.8 \pm .05 \times 10^{-14}\,\mathrm{cm}^3/\mathrm{s}$, indicating that CF_2 is lost through a two-body gas-phase addition process. This value is slightly lower than that found by other researchers.[51] This is possibly due to error in IR cross-sectional values or temperature differences within the gas. For the exothermic reaction to occur in the gas phase, the excess energy must be contained in vibrating bonds in the product molecule. Equation (18) has a standard enthalpy of $-262.4\,\mathrm{kJ/mol}$, meaning that an additional 2.7 eV must be placed in the C–F stretch bonds. This standard enthalpy can be reduced if single bonded C_2F_4 radical is produced so that only 0.6 eV of vibrational energy is stored in the product.[52] This energy can easily be stored until a photon is emitted or collision quenches.

Returning to Eq. (15), the remaining terms can be combined into a net gain as in the following:

$$G_{\mathrm{net}} = G_{\mathrm{wall}} + G_{\mathrm{react}} - L_{\mathrm{wall}}. \tag{20}$$

The gain and loss rates as functions of residence time, pressure, and power are plotted in Fig. 19. Although the combined error bars are large, a few conclusions can be drawn from the gain and loss rates. First, in a plasma system with a large ballast volume, the above-described gas-phase addition reaction dominates the loss process for CF_2. This is important because this process is frequently neglected in modeling because of the small cross section.

Second, the remaining net gain is similar in magnitude to the gain from electron impact processes. Most models only account for CF_2 production through electron impact dissociation of c-C_4F_8 and its daughter species. However, the continuity equation suggests that other processes are at least equally as important. Recently, it has been suggested that large quantities of CF_2 are produced at the walls.[26] The source of this production can be found by examining CF_2

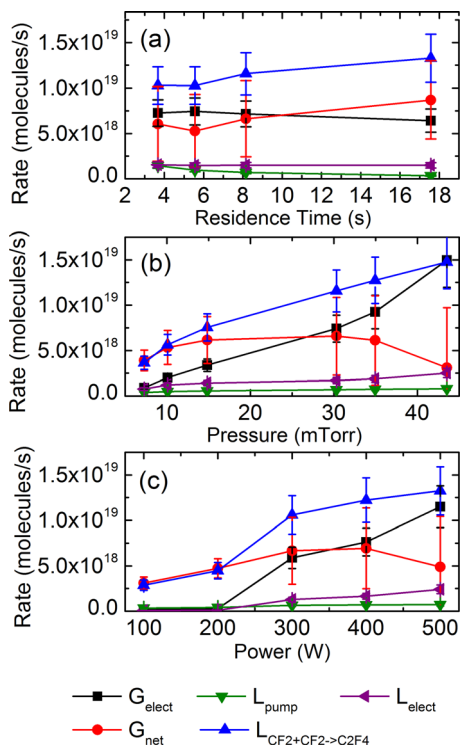

FIG. 19. (Color online) Calculated production and loss rates for CF_2 as functions of (a) residence time, (b) pressure, and (c) power.

densities in a CF_4 plasma, under clean and seasoned conditions. The highly polymerizing nature of a c-C_4F_8 plasma creates thick fluorocarbon layers very quickly. These rates can range from 200 nm/min to more than 1 μm/min depending on the proximity at room temperature,[53] making it impossible to accurately measure steady-state CF_2 densities in a "clean" chamber. However, because of the high fluorine densities in CF_4 plasmas, deposition rates are either very slow (<100 nm/min) or self-limiting to a mixing layer depth (<1 nm).[54] Thus, a chamber seasoned by 30 min in a c-C_4F_8 plasma can be exposed to a CF_4 plasma and compared to a similar plasma discharge in a clean chamber to show the influence on the plasma from the film on the walls. A 30 mTorr, 400 W plasma was used with a 30 SCCM CF_4 flow rate. As seen in Fig. 20, the steady-state CF_2 density in a clean chamber is below the detection limit of the FTIR, while the CF_2 density of 3.8×10^{13} cm^{-3} is 70% of the value measured in a c-C_4F_8 plasma. This indicates that a major source of CF_2 production is desorption from fluorocarbon films. The net gain rates calculated in Fig. 19 do not change significantly with pressure or power, while the ion flux does. This could be due to errors in the dissociation rates. However, it is also likely that other loss processes become more prominent at higher pressures and powers. Both loss to the surface and loss to reactions with fluorine would increase with pressure and power.

D. C_2F_4 production and loss mechanisms

Like those of CF_2, the gain and loss mechanisms of C_2F_4 in c-C_4F_8 plasmas have been a subject of debate. Most researchers have concluded that C_2F_4 is primarily produced from electron impact dissociation of c-C_4F_8.[55] While some have concluded that it is primarily lost by electron impact dissociation to form CF_2,[55] others have concluded that it acts as a prominent precursor to deposition on surfaces bombarded with ions at low energy[20] or as a direct etchant under higher ion energy conditions.[24] A summation of the important processes is considered in the following:

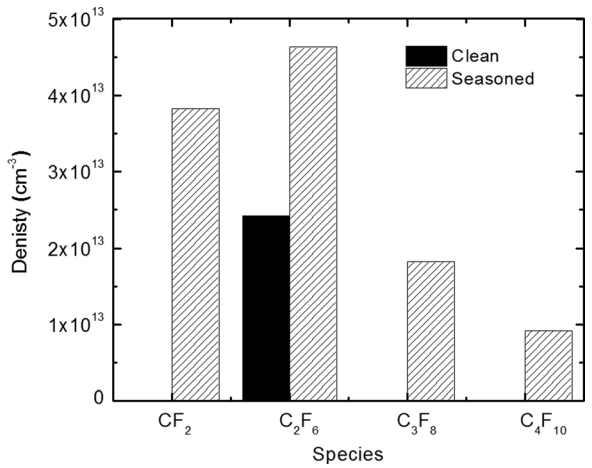

FIG. 20. Species densities in CF_4 plasmas starting with clean and seasoned conditions.

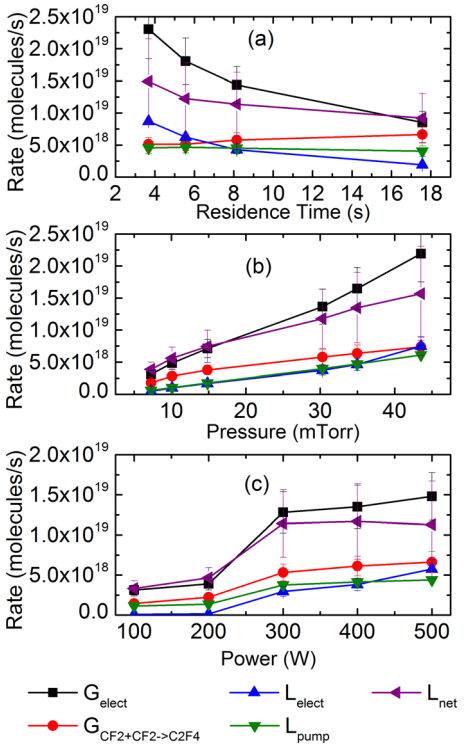

FIG. 21. (Color online) Calculated production and loss rates for C_2F_4 as functions of (a) residence time, (b) pressure, and (c) power.

$$\frac{d[C_2F_4]}{dt} = G_{elect} + G_{wall} + G_{react} - L_{elect} - L_{pump} - L_{wall} - L_{react} = 0. \quad (21)$$

Gain and loss processes for electron impact dissociation and losses to the pump can be defined as previously. Additionally, the gain rate from CF_2 addition reactions is known. Other gas-phase and wall reactions are unknown and can be combined to form a net loss,

$$L_{net} = -G_{wall} - G_{react} + L_{wall} + L_{react} = 0. \quad (22)$$

The defined gain and loss terms are plotted in Fig. 21 as functions of residence time, pressure, and power, respectively. Although the CF_2 concatenation reaction provides a significant source for C_2F_4, the main source remains electron impact dissociation of the parent gas. At low pressures the magnitude of the two gain rates becomes almost equivalent. Most significant is the magnitude of the unidentified loss. Losses to the pump and to electron impact dissociation form only a small fraction of the total loss rate of C_2F_4. This loss rate is constant within error as a function of residence time, while it increases linearly with pressure. It is impossible with the current data to identify the source of the loss. However, it remains possible that it is lost both to the wall as a precursor for deposition and to concatenation reactions with CF_2 and F to form stable neutral species such as C_2F_5, C_3F_8, and C_4F_{10}.

IV. CONCLUSION

Significant advances have been made in FTIR spectral interpretation leading to the determination of quantified gain and loss rates for neutral species in c-C_4F_8 discharges. CF_4, C_2F_6, C_3F_8, and C_4F_{10} were found to share related gain channels, likely coming off of the surface. In addition, it was found that the ratio between the gain rates of these species is dependent on the ratio of $[C_{\bar{x}}F_{2\bar{x}}]/[C_{\bar{y}}F_{2\bar{y}+1}]$ molecules either at the surface or in the gas phase. CF_2 was sourced equally through electron impact dissociation and from the walls. Because of the large ballast volume, it was lost primarily through a slow concatenation reaction in the gas phase to form C_2F_4. A rate coefficient was calculated for this reaction by using time-resolved FTIR measurements. Finally, despite the significant formation of C_2F_4 through CF_2 concatenation reactions in the ballast area, the gain from electron impact dissociation of c-C_4F_8 was the main source of C_2F_4. C_2F_4 was also found to have an unidentified loss mechanism, conjectured to be either on the surface or through gas-phase reactions to form heavy mass neutral products.

ACKNOWLEDGMENT

This work was supported in part by a gift from Applied Materials.

[1]J. W. Coburn and H. F. Winters, J. Vac. Sci. Technol. **15**, 327 (1978).
[2]J. W. Coburn and M. Chen, J. Appl. Phys. **51**, 3134 (1980).
[3]V. M. Donnelly, D. L. Flamm, W. C. Dautremont-Smith, and D. J. Werder, J. Appl. Phys. **55**, 242 (1984).
[4]I. C. Plumb and K. R. Ryan, Plasma Chem. Plasma Process. **6**, 205 (1986).
[5]G. Kokkoris, A. Goodyear, M. Cooke, and E. Gogolides. J. Phys. D: Appl. Phys. **41**, 195211 (2008).
[6]S. P. Sant, C. T. Nelson, L. J. Overzet, and M. J. Goeckner, J. Vac. Sci. Technol. A **27**, 193 (2009).
[7]M. J. Kushner, J. Appl. Phys. **53**, 2923 (1982).
[8]H. Kazumi, R. Hamasaki, and K. Tago, Plasma Sources Sci. Technol. **5**, 200 (1996).
[9]P. R. McCurdy, K. H. A. Bogart, N. F. Dalleska, and E. R. Fisher, Rev. Sci. Instrum. **68**, 1684 (1997).
[10]N. M. Mackie, V. A. Venturo, and E. R. Fisher, J. Phys. Chem. B **101**, 9425 (1997).
[11]N. E. Capps, N. M. Mackie, and E. R. Fisher, J. Appl. Phys. **84**, 4736 (1998).
[12]E. R. Fisher, Plasma Sources Sci. Technol. **11**, A105 (2002).
[13]D. Humbird and D. B. Graves, J. Appl. Phys. **96**, 65 (2004).
[14]D. Humbird and D. B. Graves, J. Appl. Phys. **96**, 791 (2004).
[15]D. Humbird, D. B. Graves, X. F. Hua, and G. S. Oehrlein, Appl. Phys. Lett. **84**, 1073 (2004).
[16]T. E. F. M. Standaert, C. Hedlund, E. A. Joseph, G. S. Oehrlein, and T. J. Dalton, J. Vac. Sci. Technol. A **22**, 53 (2004).
[17]M. Schaepkens, R. C. M. Bosch, T. E. F. M. Standaert, G. S. Oehrlein, and J. M. Cook, J. Vac. Sci. Technol. A **16**, 2099 (1998).
[18]A. Tserepi, J. Derouard, J. P. Booth, and N. Sadeghi, J. Appl. Phys. **81**, 2124 (1997).
[19]J. P. Booth, Plasma Sources Sci. Technol. **8**, 249 (1999).
[20]H. Hayashi, S. Morishita, T. Tatsumi, Y. Hikosaka, S. Noda, H. Nakagawa, S. Kobayashi, M. Inoue, and T. Hosino, J. Vac. Sci. Technol. A **17**, 2557 (1999).
[21]E. A. Joseph, B. S. Zhou, S. P. Sant, L. J. Overzet, and M. J. Goeckner, J. Vac. Sci. Technol. A **22**, 689 (2004).
[22]B. Zhou, E. A. Joseph, L. J. Overzet, and M. J. Goeckner, J. Vac. Sci. Technol. A **24**, 114 (2006).
[23]S. P. Sant, C. T. Nelson, L. J. Overzet, and M. J. Goeckner, J. Vac. Sci. Technol. A **27**, 631 (2009).
[24]M. Barela, H. M. Anderson, and G. S. Oehrlein, J. Vac. Sci. Technol. A **23**, 408 (2005).
[25]G. Cunge and J. P. Booth, J. Appl. Phys. **85**, 3952 (1999).
[26]J. P. Booth, H. Abada, P. Chabert, and D. B. Graves, Plasma Sources Sci. Technol. **14**, 273 (2005).
[27]H. H. Doh and Y. Horike, J. Vac. Sci. Technol. A **20**, 1420 (2002).
[28]A. Milella, F. Palumbo, P. Favia, G. Cicala, and R. d'Agostino, Pure Appl. Chem. **77**, 399 (2005).
[29]K. Takahashi, A. Itoh, T. Nakamura, and K. Tachibana, Thin Solid Films **374**, 303 (2000).
[30]M. Haverlag, E. Stoffels, W. W. Stoffels, G. M. W. Kroesen, and F. J. de Hoog, J. Vac. Sci. Technol. A **12**, 3102 (1994).
[31]K. Iinuma, N. Sasaki, T. Takahashi, M. Fujisawa, J. Suzuki, K. Satoh, K. Furukawa, and Y. Satoh, Rev. Sci. Instrum. **68**, 2305 (1997).
[32]J. O'Neill, J. Singh, and G. Gifford, J. Vac. Sci. Technol. A **8**, 1716 (1990).
[33]H. U. Poll, D. Hinze, and H. Schlemm, Appl. Spectrosc. **36**, 445 (1982).
[34]C. T. Nelson, "Gain and loss mechanisms in fluorocarbon plasmas," Ph.D. dissertation (University of Texas at Dallas, 2010).
[35]M. J. Goeckner, J. M. Marquis, B. J. Markham, A. K. Jindal, E. A. Joseph, and B. Zhou, Rev. Sci. Instrum. **75**, 884 (2004).
[36]C. Y. Duluard, R. Dussart, T. Tillocher, L. E. Pichon, P. Lefaucheux, M. Puech, and P. Ranson, Plasma Sources Sci. Technol. **17**, 045008 (2008).
[37]S. E. Savas, Appl. Phys. Lett. **48**, 1042 (1986).
[38]S. B. Radovanov, B. Tomčik, Z. Lj. Petrović, and B. M. Jelenković, J. Appl. Phys. **67**, 97 (1990).
[39]T. Kimura and K. Hanaki, Jpn. J. Appl. Phys. **47**, 8546 (2008).
[40]M. H. Lee, S. H. Jang, and C. W. Chung, J. Appl. Phys. **101**, 033305 (2007).
[41]J. U. White, J. Opt. Soc. Am. **32**, 285 (1942).
[42]C. T. Nelson, L. J. Overzet, and M. J. Goeckner, J. Vac. Sci. Technol. A **30**, 021305 (2012).
[43]M. A. Lieberman and A. J. Lichtenberg, *Principles of Plasma Discharges and Material Processing*, 2nd ed. (Wiley, Hoboken, NJ, 2005).
[44]L. G. Christophorou and J. K. Olthoff, J. Phys. Chem. Ref. Data **28**, 967 (1999).
[45]D. W. Flaherty, M. A. Kasper, J. E. Baio, D. B. Graves, H. F. Winters, C. Winstead, and V. McKoy, J. Phys. D: Appl. Phys. **39**, 4393 (2006).
[46]J. E. Baio, H. Yu, D. W. Flaherty, H. F. Winters, and D. B. Graves, J. Phys. D: Appl. Phys. **40**, 6969 (2007).
[47]K. Yoshida, S. Goto, H. Tagashira, C. Winstead, and B. McKoy, J. Appl. Phys. **91**, 2637 (2002).
[48]L. G. Christophorou and J. K. Olthoff, J. Phys. Chem. Ref. Data **30**, 449 (2001).
[49]G. I. Font, W. L. Morgan, and G. Mennega, J. Appl. Phys. **91**, 3530 (2002).
[50]D. M. Lemal, J. Org. Chem. **69**, 1 (2004).
[51]S. Sharpe, B. Harnett, H. S. Sethi, and D. S. Sethi, J. Photochem. **38**, 1 (1987).
[52]N. N. Buravstev and Yu. A. Kolbanovskii, Russ. J. Appl. Chem. **75**, 598 (2002).
[53]C. T. Nelson, S. P. Sant, L. J. Overzet, and M. J. Goeckner, Plasma Sources Sci. Technol. **16**, 813 (2007).
[54]N. R. Rueger, J. J. Beulens, M. Schaepkens, M. F. Doemling, J. M. Mirza, T. E. F. M. Standaert, and G. S. Oehrlein, J. Vac. Sci. Technol. A **15**, 1881 (1997).
[55]S. Rauf and P. L. G. Ventzek, J. Vac. Sci. Technol. A **20**, 14 (2002).